COMMUNICATION

Check for updates

Unlocking ferroelectricity in a metal-free adamantane derivative *via* targeted symmetry reduction†

Wei-Jian Xu, [ID] *[ab] Denis Alikin,[c] Zi-Luo Fang,[a] Konstantin Romanyuk,[c]
Luis Verissimo,[b] Pavel Zelenovskii,[c] Wei-Xiong Zhang, [ID] *[a] Andrei Kholkin [ID] *[cd]
and João Rocha [ID] *[b]

By introducing a symmetry-reduction design strategy in adamantane derivatives, overcoming the inherent high symmetry of globular molecules that typically hinders long-range electrical ordering, we report a metal-free ferroelectric 2-adamantylammonium bromide (2-ADAB) with a high Curie temperature of 383 K and robust polarization switching.

Metal-free ferroelectrics, composed of organic or molecular components, have emerged as promising alternatives to conventional metal-containing counterparts for applications in areas such as biomedicine, flexible electronics, and wearable technologies, primarily due to their cost-effectiveness, lightweight nature, and biocompatibility.[1–4] Beyond these intrinsic advantages, metal-free ferroelectrics provide greater flexibility in design, enabling the precise tailoring of properties such as ferroelectricity,[5] antiferroelectricity,[6] piezoelectricity,[7] dielectric response,[8] and photovoltaic properties through targeted structural modifications.[9] Such tailored control over material functionality has been made increasingly feasible through recent advances in molecular design strategies,[10] computational modelling,[11] and data mining from the Cambridge Structural Database. Notably, these interdisciplinary approaches have accelerated the discovery of high-performance metal-free ferroelectrics, as exemplified by (*N*-methyl-*N'*-diazabicyclo[2.2.2]octonium)NH$_4$I$_3$,[12] (*N*-methyl-*N'*-diazabicyclo[2.2.2]octonium)NH$_4$(PF$_6$)$_3$,[13] and (*N*-chloromethyl-*N'*-diazabicyclo[2.2.2]octonium)NH$_4$(ClO$_4$)$_3$.[14]

[a] MOE Key Laboratory of Bioinorganic and Synthetic Chemistry, School of Chemistry, IGCME, Sun Yat-Sen University, Guangzhou 510275, China. E-mail: xuweijian@mail.sysu.edu.cn, zhangwx6@mail.sysu.edu.cn

[b] Department of Chemistry & CICECO-Aveiro Institute of Materials, University of Aveiro, 3810-193 Aveiro, Portugal. E-mail: rocha@ua.pt

[c] Department of Physics & CICECO-Aveiro Institute of Materials, University of Aveiro, 3810-193 Aveiro, Portugal. E-mail: kholkin@ua.pt

[d] Institute of Solid State State Physics, University of Latvia, LV-1063 Riga, Latvia. E-mail: andrei.kholkin@cfi.lu.lv

† Electronic supplementary information (ESI) available: The experimental details and characterization. CCDC 2345092–2345094. For ESI and crystallographic data in CIF or other electronic format see DOI: https://doi.org/10.1039/d5cc01790d

Particularly, the recent discovery of metal-free plastic ferroelectric crystals composed of globular molecules has highlighted the unique potential of spherical molecular systems in addressing the limitations of conventional ferroelectrics.[15] These molecular systems, as exemplified by quinuclidine,[16,17] 1,4-diazabicyclo[2.2.2]octane,[18,19] and carborane derivatives,[20,21] possess inherently low rotational energy barriers, enabling order–disorder ferroelectric transitions and facilitating polarization switching at low coercive fields.[22,23] Additionally, their high initial symmetry in the paraelectric phase allows for pronounced symmetry breaking during phase transitions, leading to ferroelectric phases with multiple polarization directions.[24,25] However, the inherent high symmetry of globular molecules thermodynamically favours antiparallel dipole arrangements, stabilizing centrosymmetric crystal packing—a structural motif fundamentally incompatible with the noncentrosymmetric lattice symmetry prerequisite for ferroelectricity. Consequently, the design and synthesis of new metal-free ferroelectrics based on globular molecules remain a significant challenge, particularly for achieving high Curie temperatures and robust reversible polarization.[26]

To this end, the adamantane molecule (T_d symmetry, C$_{10}$H$_{16}$), a prototypical diamondoid, serves as an ideal model system for symmetry engineering for causing ferroelectricity.[27,28] While its inherent high symmetry typically enforces centrosymmetric packing, the rigid yet chemically modifiable cage structure allows targeted symmetry reduction through strategic functionalization.[29,30] By strategically introducing polar functional groups at specific vertices, we aim to reduce molecular symmetry and disrupt inversion centres, thereby stabilizing noncentrosymmetric polar phases. This approach is anticipated to "unlock" ferroelectricity in adamantane derivatives, harnessing the inherent rigidity of the spherical cage structure to stabilize ordered dipole alignment, while its low rotational energy barrier facilitates polarization reversal under external electric fields.

Herein, we present a symmetry-reduction strategy to induce ferroelectricity in adamantane derivatives (Fig. 1). Specifically, protonation of amine-functionalized adamantane generates

Fig. 1 Stepwise symmetry-reduction strategy for the synthesis of 2-adamantyl-ammonium bromide (2-ADAB). The approach involves strategic ionization of high-symmetry adamantane and precise modification of the amine group position to lower molecular symmetry.

1-adamantylammonium (C_{3v}-symmetric), which crystallizes as centrosymmetric 1-adamantylammonium bromide (1-ADAB). Structural isomerization through amine repositioning produced 2-adamantylammonium (C_s-symmetric), forming 2-adamantyl-ammonium bromide (2-ADAB). The reduced symmetry disrupts inversion centres, stabilizing a polar structure. Notably, the structural design endows 2-ADAB with robust polarization switching and a high Curie temperature of 383 K, demonstrating the effectiveness of the symmetry-reduction strategy in achieving ferroelectricity. The ferroelectric mechanism and properties of 2-ADAB were investigated systematically through thermal analysis, variable-temperature single-crystal X-ray diffraction,

dielectric spectroscopy, second harmonic generation (SHG), and piezoresponse force microscopy (PFM).

Single crystal X-ray diffraction analysis revealed that 1-ADAB crystallizes in the centrosymmetric space group of $P2_1/n$ at 298 K (Table S1, ESI†). Each 1-adamantylammonium cation interacts with Br⁻ anions *via* weak intermolecular N–H···Br hydrogen bonds (Table S2, ESI†), resulting in an antiparallel arrangement that cancels the unit cell's dipole moment, thus preventing ferroelectricity (Fig. S3, ESI†). Conversely, 2-ADAB crystallizes in a polar space group, $P2_1$, in the ferroelectric phase (FP) at 298 K with a 2-adamantylammonium cation and a single Br anion in the asymmetric unit. The hydrogen bonds formed between 2-adamantylammonium cations and Br anions (ranging from 3.309 to 3.456 Å, Table S3, ESI†) foster a polar alignment, which, in turn, induces a spontaneous polarization along the b axis (Fig. 2a). At 393 K, in the paraelectric phase (PP), 2-ADAB adopts the centrosymmetric monoclinic space group $P2_1/m$, featuring halves of 2-adamantylammonium cations and Br⁻ anions in the asymmetric unit. Specifically, both cations and anions lie on the mirror symmetry plane, creating a centrosymmetric structure characteristic of the PP (Fig. 2b and Fig. S4, ESI†). Therefore, the PP-to-FP transition reduces the symmetry elements of the crystallographic point group from 4 (E, C_2, i, m) to 2 (E, C_2), indicating symmetry breaking. This process, described by the Aizu notation of 2/mF2, is characteristic of ferroelectric transitions.[31]

Differential scanning calorimetry (DSC) showed that 2-ADAB undergoes a reversible phase transition near T_c = 383 K upon heating, with a corresponding exothermic peak observed at around 381 K during the cooling process (Fig. 3a). The entropy change, ΔS, calculated from the DSC curve, is estimated to be 1.34 J mol⁻¹ K⁻¹. By applying the Boltzmann equation, $\Delta S = R \ln(N)$, where N is the ratio of the number of states between the different phases and R is the gas constant, the derived value of N at 1.2 indicates a subtle structural change during the phase transition, consistent with the structural analysis. The narrow thermal hysteresis of 2 K and broad DSC peaks suggest a second-order ferroelectric phase transition.

The symmetry-breaking ferroelectric phase transition was unambiguously confirmed by temperature-dependent SHG measurements. As depicted in Fig. 3b, the SHG intensity progressively diminishes upon heating, ultimately dropping to the noise floor above T_c = 383 K, while the cooling cycle restores the signal to its initial magnitude. This observation aligns with a reversible
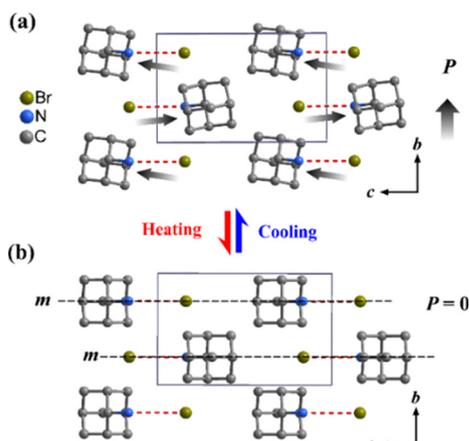
Fig. 2 Crystal structure of (a) ferroelectric and (b) paraelectric phases of 2-ADAB at 298 K and 393 K, respectively. Hydrogen atoms are omitted for clarity.
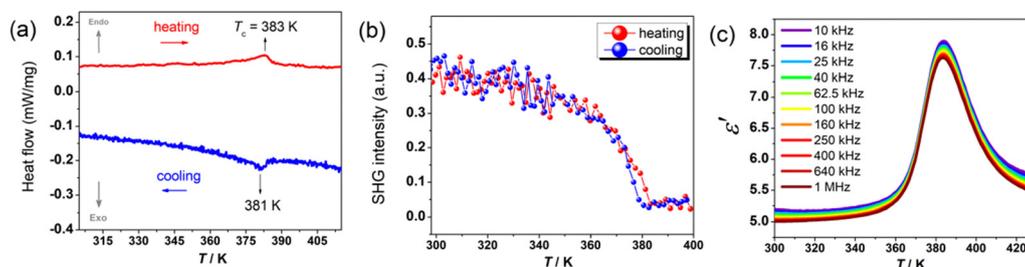
Fig. 3 Thermal, optical, and dielectric properties of 2-ADAB. (a) DSC curves showing a reversible phase transition near 383 K. (b) Temperature-dependent SHG intensity, confirming the noncentrosymmetric nature of ferroelectric phase. (c) The temperature-dependent dielectric constant (ε') measured on a pressed-powder pellet during the heating run.
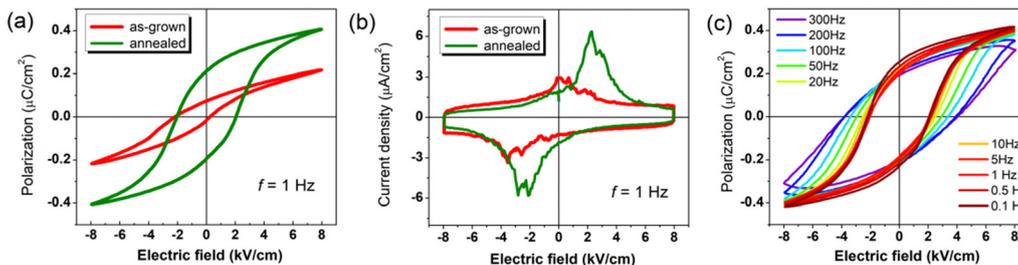
Fig. 4 Polarization switching behaviour of 2-ADAB single crystals. (a) P–E hysteresis loops for the as-grown state and the annealed states at 298 K (b) Current density–electric field curves. (c) Frequency-dependent P–E hysteresis loops for annealed sample measured under an applied electric field.

structural transition between the noncentrosymmetric FP and the centrosymmetric PP.

The temperature-dependent dielectric constant (ε') of 2-ADAB, measured over a broad frequency range (10 kHz–1 MHz), exhibits a sharp increase from ~ 5.0 at 300 K to a peak of ~ 7.6 at T_c of 383 K, followed by a decrease to ~ 5.4 at 430 K during the heating process (Fig. 3c and Fig. S6, ESI†). The dielectric anomaly, marked by a λ peak around T_c, is characteristic of a proper ferroelectric phase transition. In situ measurements during the cooling run reconfirmed the reversibility of the dielectric anomaly (Fig. S7, ESI†).

The polarization–electric field (P–E) hysteresis loops of 2-ADAB were measured on a single crystal sample along the b-axis, i.e., the polar axis. The as-grown sample exhibited a remnant polarization of $P_r \sim 0.07$ μC cm^{-2}. After 5 minutes of annealing the crystal at 120 °C under isothermal conditions with subsequent natural cooling, the remnant polarization increased to $P_r \sim 0.21$ μC cm^{-2} (Fig. 4a). This enhancement aligns with the theoretically predicted saturated polarization (0.23 μC cm^{-2}) from quantum chemical calculations (ESI†), where the reduced P_r reflects domain-wall pinning effects in the as grown state.[32] Furthermore, the current density-electric field curve, exhibits two distinct peaks, indicative of the presence of two stable states with opposing polarizations (Fig. 4b). Fig. 4c presents frequency-dependent hysteresis loops under an 8 kV cm^{-1} electric field at room temperature. As the frequency decreases from 300 to 0.1 Hz, the P_r increases from 0.19 to 0.25 μC cm^{-2}, while the coercive field (E_c) decreases from 3.8 to 2.2 kV cm^{-1}. Combining high T_c, low E_c, and robust polarization-switching capability, 2-ADAB demonstrates a potential for low-power flexible electronic devices.

PFM analysis of drop-coated 2-ADAB thin films revealed crystallized topographic planes, with powder XRD confirming predominant (001)-oriented growth (Fig. S8–S10a, ESI†), indicative of in-plane polarization. Both vertical and lateral PFM measurements (Fig. S10b–e, ESI†) demonstrated randomly distributed ferroelectric domains, showing no correlation between domain patterns and surface morphology. Notably, distinct phase and amplitude contrasts between vertical PFM and lateral PFM suggest non-180° domain walls, which are inconsistent with the uniaxial ferroelectricity of 2-ADAB. These deviations, akin to relaxor ferroelectrics or morphotropic phase boundary phenomena, likely originate from structural irregularities such as defects, impurities, or compositional heterogeneity within the crystal lattice.[33]
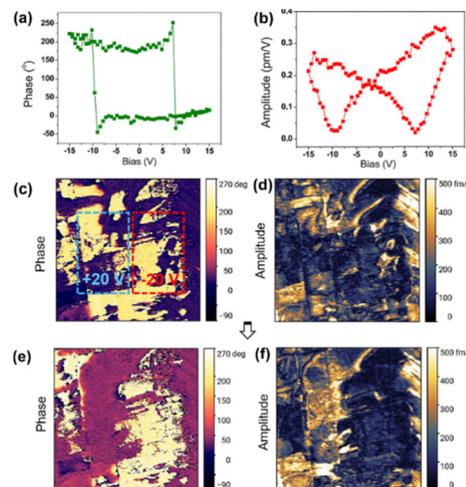

Fig. 5 Local polarization switching in drop-coated 2-ADAB films. (a) Phase-voltage hysteresis loop and (b) amplitude-voltage butterfly loop obtained via PFM. Vertical PFM images showing (c) phase and (d) amplitude before poling, and (e) phase and (f) amplitude after local poling with ±20 V bias.

To probe the polarization reversal characteristics, the phase and amplitude were measured by sweeping the applied tip voltage from −15 V to 15 V. As shown in Fig. 5a, the PFM phase signal exhibits a sharp 180° reversal upon surpassing the asymmetric coercive voltages of −9 V (negative bias) and +7 V (positive bias). Simultaneously, Fig. 5b reveals butterfly-shaped amplitude hysteresis loops, with strain modulation evident across the entire voltage range (±15 V). Collectively, these findings serve as unambiguous indicators of polarization switching in the 2-ADAB thin film. The shape of these local piezoresponse hysteresis loops resembles that of the macroscopic P–E loops, indicating a considerable degree of back-switching of the polarization (Fig. S11, ESI†). Local domain switching was performed within a bi-polar square area of the film using a biased probe in motion. As depicted in Fig. 5c–f, upon applying +20 V and −20 V voltages, the vertical PFM phase and amplitude images reveal remarkable changes in domain structures. The distinct contrast variations in phase images and corresponding amplitude responses under external electric fields confirm that polarization reversal and change of domain structure, providing direct evidence of microscale ferroelectric properties.

By implementing a symmetry-reduction strategy in adamantane derivatives, we successfully engineered 2-ADAB, a metal-free ferroelectric crystal that undergoes a FP-to-PP phase transition at a high temperature of 383 K. Moreover, 2-ADAB exhibits robust polarization switching with a relatively low E_c of 2.2 kV cm^{-1} and a noticeable remnant polarization of 0.21 μC cm^{-2} at room temperature. This work establishes symmetry engineering as an effective strategy to disrupt centrosymmetry in globular molecular systems, enabling ferroelectricity in rigid spherical architectures beyond adamantane derivatives and advancing the development of high-performance metal-free ferroelectrics.

Data availability

Crystallographic data have been deposited with CCDC number 2345092–2345094 can be obtained from https://www.ccdc.cam.ac.uk. The remaining data supporting this article have been included as part of the ESI.†

Conflicts of interest

There are no conflicts to declare.

Notes and references

1 H.-Y. Zhang, Y.-Y. Tang, Z.-X. Gu, P. Wang, X.-G. Chen, H.-P. Lv, P.-F. Li, Q. Jiang, N. Gu, S. Ren and R.-G. Xiong, Science, 2024, 383, 1492–1498.
2 A. S. Tayi, A. Kaeser, M. Matsumoto, T. Aida and S. I. Stupp, Nat. Chem., 2015, 7, 281–294.
3 S. Horiuchi and Y. Tokura, Nat. Mater., 2008, 7, 357–366.
4 M. Owczarek, K. A. Hujsak, D. P. Ferris, A. Prokofjevs, I. Majerz, P. Szklarz, H. Zhang, A. A. Sarjeant, C. L. Stern, R. Jakubas, S. Hong, V. P. Dravid and J. F. Stoddart, Nat. Commun., 2016, 7, 13108.
5 H.-Y. Zhang, Chem. Sci., 2022, 13, 5006–5013.
6 H. Xu, W. Guo, J. Wang, Y. Ma, S. Han, Y. Liu, L. Lu, X. Pan, J. Luo and Z. Sun, J. Am. Chem. Soc., 2021, 143, 14379–14385.
7 S. Guerin, A. Stapleton, D. Chovan, R. Mouras, M. Gleeson, C. McKeown, M. R. Noor, C. Silien, F. M. F. Rhen, A. L. Kholkin, N. Liu, T. Soulimane, S. A. M. Tofail and D. Thompson, Nat. Mater., 2018, 17, 180–186.
8 C. Shi, X. Zhang, C.-H. Yu, Y.-F. Yao and W. Zhang, Nat. Commun., 2018, 9, 481.
9 S. Jiao, H. Jiang, C. Fan, C. Xu, J. Jiang, Y. Xu, Z. Tang, X. Sun, P. Ji, X. Yang, K. Ye, L. Xu, Q. You, S. Chen, H.-L. Cai and X. Wu, Chem. Eng. J., 2023, 477, 146805.
10 X. Mu, H.-Y. Zhang, L. Xu, Y.-Y. Xu, H. Peng, Y.-Y. Tang and R.-G. Xiong, APL Mater., 2021, 9, 051112.
11 H. Liu, Y. Ye, X. Zhang, T. Yang, W. Wen and S. Jiang, J. Mater. Chem. C, 2022, 10, 13676–13689.
12 H.-Y. Ye, Y.-Y. Tang, P.-F. Li, W.-Q. Liao, J.-X. Gao, X.-N. Hua, H. Cai, P.-P. Shi, Y.-M. You and R.-G. Xiong, Science, 2018, 361, 151–155.
13 H. S. Choi, S. Li, I.-H. Park, W. H. Liew, Z. Zhu, K. C. Kwon, L. Wang, I.-H. Oh, S. Zheng, C. Su, Q.-H. Xu, K. Yao, F. Pan and K. P. Loh, Nat. Commun., 2022, 13, 794.
14 Z.-X. Zhang, H.-F. Ni, J.-S. Tang, P.-Z. Huang, J.-Q. Luo, F.-W. Zhang, J.-H. Lin, Q.-Q. Jia, G. Teri, C.-F. Wang, D.-W. Fu and Y. Zhang, J. Am. Chem. Soc., 2024, 146, 27443–27450.
15 J. Harada, T. Shimojo, H. Oyamaguchi, H. Hasegawa, Y. Takahashi, K. Satomi, Y. Suzuki, J. Kawamata and T. Inabe, Nat. Chem., 2016, 8, 946–952.
16 P.-F. Li, W.-Q. Liao, Y.-Y. Tang, W. Qiao, D. Zhao, Y. Ai, Y.-F. Yao and R.-G. Xiong, Proc. Natl. Acad. Sci. U. S. A., 2019, 116, 5878–5885.
17 X.-M. Zhao, D. Li, H.-X. Zhao, Y.-P. Ren, L.-S. Long and L.-S. Zheng, Inorg. Chem., 2020, 59, 5475–5482.
18 P.-P. Shi, Y.-Y. Tang, P.-F. Li, H.-Y. Ye and R.-G. Xiong, J. Am. Chem. Soc., 2017, 139, 1319–1324.
19 J.-Y. Li, Q.-L. Xu, S.-Y. Ye, L. Tong, X. Chen and L.-Z. Chen, Chem. Commun., 2021, 57, 943–946.
20 W. Guo, Z. Yang, L. Shu, H. Cai and Z. Wei, Angew. Chem., Int. Ed., 2024, 63, e202407934.
21 D. A. Gruzdev, A. S. Nuraeva, P. A. Slepukhin, G. L. Levit, P. S. Zelenovskiy, V. Y. Shur and V. P. Krasnov, J. Mater. Chem. C, 2018, 6, 8638–8645.
22 Y.-X. Zhao, K.-G. Gao, Z.-S. Yao and J. Tao, Inorg. Chem., 2023, 62, 8778–8783.
23 X.-J. Song, Z.-X. Zhang, X.-G. Chen, H.-Y. Zhang, Q. Pan, J. Yao, Y.-M. You and R.-G. Xiong, J. Am. Chem. Soc., 2020, 142, 9000–9006.
24 H. Morita, R. Tsunashima, S. Nishihara, K. Inoue, Y. Omura, Y. Suzuki, J. Kawamata, N. Hoshino and T. Akutagawa, Angew. Chem., Int. Ed., 2019, 58, 9184–9187.
25 Y. Xie, Y. Ai, Y.-L. Zeng, W.-H. He, X.-Q. Huang, D.-W. Fu, J.-X. Gao, X.-G. Chen and Y.-Y. Tang, J. Am. Chem. Soc., 2020, 142, 12486–12492.
26 Y. Ai, W.-Q. Liao, Y.-R. Weng, H.-P. Lv, X.-G. Chen, X.-J. Song, P.-F. Li and R.-G. Xiong, J. Am. Chem. Soc., 2023, 145, 23292–23299.
27 H. Schwertfeger, A. A. Fokin and P. R. Schreiner, Angew. Chem., Int. Ed., 2008, 47, 1022–1036.
28 Y.-A. Xiong, Z.-X. Gu, X.-J. Song, J. Yao, Q. Pan, Z.-J. Feng, G.-W. Du, H.-R. Ji, T.-T. Sha, R.-G. Xiong and Y.-M. You, J. Am. Chem. Soc., 2022, 144, 13806–13814.
29 L. Yuan, S. Clevers, A. Burel, P. Negrier, M. D. Barrio, B. Ben Hassine, D. Mondieig, V. Dupray, J. L. Tamarit and G. Coquerel, Cryst. Growth Des., 2017, 17, 3395–3401.
30 K. Abdur-Rashid, S. Saha, J. Mugisha, S. Teale, S. Wang, M. Saber, A. Lough, E. Sargent and U. Fekl, Chem. – Eur. J., 2024, e202302998.
31 K. Aizu, J. Phys. Soc. Jpn., 1969, 27, 387–396.
32 F. Kagawa, S. Horiuchi, N. Minami, S. Ishibashi, K. Kobayashi, R. Kumai, Y. Murakami and Y. Tokura, Nano Lett., 2014, 14, 239–243.
33 D. Alikin, A. Abramov, A. Turygin, A. Ievlev, V. Pryakhina, D. Karpinsky, Q. Hu, L. Jin, V. Shur, A. Tselev and A. Kholkin, Small Methods, 2022, 6, 2101289.